OPEN ACCESS
JOURNAL OF ADVANCED DIELECTRICS
Vol. 12, No. 5 (2022) 2244005 (11 pages)

DOI: 10.1142/S2010135X22440052

Crystal structure, microstructure, electrophysical properties, and thermally induced aging of PZT-$CdNb_2O_6$ ceramics

Andryushin Konstantin*, Pavelko Alexey*, Sahoo Sushrisangita*, Shilkina Lidiya*, Nagaenko Alxandr†, Andryushina Inna*,‡, Moysa Maksim* and Reznichenko Larisa*

*Research Institute of Physics, Southern Federal University
Rostov-on-Don, 344090, Stachki str. 194, Russia

†Institute of High Technology and Piezo Technic, Southern Federal University
Rostov-on-Don, 344090, Milchakova 10, Russia

‡kpandryushin@gmail.com

Received 3 June 2022; Revised 20 July 2022; Accepted 7 August 2022; Published 2 September 2022

Solid solution samples of the three-component system $(1 - x)Pb(Ti_{0.5}Zr_{0.5})O_3–xCdNb_2O_6$ with $x = 0.0125–0.0500$, $\Delta x = 0.0125$ were obtained by solid phase synthesis followed by sintering using conventional ceramic technology. The crystal structure, microstructure, electrophysical, and thermophysical properties of these ceramics have been studied. It is shown that all studied solid solutions can be divided into two groups (with $x = 0.0125$ and with $x > 0.0125$), characterized by different characteristics of the change in properties with variations in external influences. This is probably due to the transition from a perovskite-type structure with a tetragonal (T) unit cell to inhomogeneous solid solutions consisting of a series of T-phases with similar cell parameters. A conclusion is made about the expediency of using the data obtained in the development of similar materials for devices based on them.

Keywords: PZT; $CdNb_2O_6$; XRD; microstructure; piezoelectric properties; thermophysical properties; phase transition fatigue.

1. Introduction

Piezoelectric ceramic materials over the past 70 years have found wide application in various fields related to both daily human life and various stages of industrial production.[1,2] The overwhelming majority of such piezoactive ceramics are based on solid solutions (SS) based on the lead zirconate-titanate ($PbZr_{1-x}Ti_xO_3$, PZT) system.[2,3] However, the ever-growing requirements for the electrical properties of such materials have practically exhausted the possibilities of this basic composition. And this forces many scientific groups to carry out work to improve manufacturability and expand the range of parameter sets implemented in ceramics based on them. One of the possible ways to solve the described problem is to design three-component systems by introducing, for example, nonisostructural components into the basic SS PZT. A possible candidate is cadmium niobate ($CdNb_2O_6$), which has the columbite structure[4,5] and is used in optoelectronics.[6,7] In materials developed by this method, the range of compositions with various properties can be significantly expanded and, as a result, the possibilities for the practical application of such media will expand.

Since the materials being developed often operate under critical conditions for them (as a rule, the external temperature varies in fairly wide ranges), the question of the behavior of the electrical and thermal properties in the range from room temperature to the phase transition to the nonpolar state arises. Furthermore, given the duration of operation of devices under these conditions, information about the possible degradation of properties is required. The solution of this problem is possible through the formation of artificial thermally induced aging.

Therefore, the development of a three-component system based on nonisostructural components of PZT SS and the compound $CdNb_2O_6$, the establishment of composition–structure–property correlations in a wide range of external influences, which became the goal of this work, is topical.

2. Materials and Methods

2.1. *Fabrication of samples*

The objective of the study was the SS based on the system $(1 - x)PbTi_{0.5}Zr_{0.5}O_3 - xCdNb_2O_6$ with $x = 0.0125–0.0500$, $\Delta x = 0.0125$. $NaHCO_3$ — 99%, Nb_2O_5 — 99%, CdO — 99%, PbO, ZrO_2 — 99%, TiO_2 — 99.8% were used as raw materials. The samples were obtained by solid-phase synthesis in two stages and sintered according to conventional ceramic technology with hot forming elements, when external pressure is applied for a short time to the sintered workpiece at the moment of the highest plastic flow rate, i.e., at a temperature of ~0.7 $T_{opt.}$ ($T_{opt.}$ is the optimal sintering temperature, $T_{sint.}$).

‡Corresponding author.

The time of action of the applied pressure is ~0.5 h. Such a procedure should ensure the testing of the microstructure of ceramics and the improvement of their macroresponses: $T_{synt.1}$ = 1170K, $\tau_{synt.1}$ = 4 h, $T_{synt.2}$ = 1220K, $\tau_{synt.2}$ = 10 h, $T_{sint.}$ = 1490K, depending on composition.

The manufacture of measuring samples included two technological operations: mechanical processing and electrode application. Search measuring samples were made in the form of disks ∅10 × 1 mm. Surface treatment was carried out with a diamond tool according to the 6th accuracy class. The electrodes were deposited on flat surfaces by double firing of silver-containing paste at a temperature of (1070 ± 20) K for 0.5 h.

2.2. *Methods of studying samples*

X-ray studies were performed by powder diffraction using DRON-3 (CoK_α radiation; Mn filter; Bragg–Brentano focus scheme). Crushed ceramic objects were studied, making it possible to exclude the influence of surface effects, stresses, and textures that arise in the process of obtaining ceramics. The structural parameters were calculated according to standard methods. The measurement errors of the structural parameters have the following values: linear $\Delta a = \Delta b = \Delta c = \pm(0.002 \div 0.004)$ Å; angular $\Delta\beta = 3'$; volume $\Delta V = \pm 0.05$Å^3 ($\Delta V/V \cdot 100\% = 0.07\%$), T-tetragonal phase, Rh- rhombohedral phase, C-cubic phase, PcC- pseudocubic (fuzzy symmetry phase), RFS- fuzzy symmetry region.

The dependences of the real and imaginary parts of the relative complex permittivity $\varepsilon^*/\varepsilon_0 = \varepsilon'/\varepsilon_0 - i\varepsilon''/\varepsilon_0$ ($\varepsilon_0 = 8.75 \times 10^{-12}$ F/m – dielectric constant) on the sample temperature at T = (300–970) K in the frequency range $f = 25 \times 10^6$ Hz was obtained using a measuring bench based on an Agilent 4980A LCR- meter. The monotonous heating and cooling regimes were 1 K/min.

Thermally induced fatigue study was carried out on the basis of data on the dependence of dielectric properties on temperature, which were obtained using a measuring bench based on an Agilent 4980A LCR meter. 35÷45 cycles of sample heating above the Curie point (T_C) and cooling by ~100K below T_C (thermal cycling) were carried out. For each cycle, separate datasets were recorded which were then analyzed. To describe the degree of smearing of the ferroelectric (FE) phase transition, we used the empirical relation,[8] which most accurately describes the temperature dependence of the dielectric constant at $T > T_m$:

$$\frac{\varepsilon_A}{\varepsilon} = 1 + \frac{(T - T_A)^2}{2\delta_A^2}, \quad (1)$$

where ε_A and T_A are some virtual values of the maximum dielectric constant and the corresponding temperature, δ_A is a measure of the degree of spreading of the dielectric peak, ε is the relative permittivity. The calculation of these parameters was carried out using a nonlinear approximation of $\varepsilon'/\varepsilon_0(T)$ curves with the help of the ALGLIB plug-in library of algorithms ALGLIB. A detailed description of the methodology is given in Ref. 9.

Measurement of the electrical parameters of the SSs at T = (300 ÷ 970)K was carried out using a precision LCR-meter Agilent 4980A by the resonance-antiresonance method,[10] while determining the relative permittivity of unpolarized ($\varepsilon/\varepsilon_0$) and polarized ($\varepsilon_{33}^T/\varepsilon_0$) samples, dielectric losses in a weak field (dielectric loss tangent, $tg\delta$), piezoelectric moduli (d_{ij}: $|d_{31}|$, d_{33}), piezoelectric coefficients (piezosensitivity) (g_{ij}: $|g_{31}|$, g_{33}), electromechanical coupling coefficient of the planar oscillation mode (K_p), mechanical quality factor (Q_M), Young′s modulus (Y_{11}^E), speed of sound (V_1^E). The measurement errors of the electrophysical parameters have the following values: $\varepsilon_{33}^T/\varepsilon_0 \le \pm 1.5\%$, $K_p \le \pm 2.0\%$, $|d_{31}| \le \pm 4.0\%$, $Q_M \le \pm 12\%$; $Y_{11}^E \le \pm 0.7\%$. The piezomodule d_{33} and, respectively, the piezoelectric coefficient g_{33} were measured at room temperature using the quasistatic method using the Piezo d_{33} Test System (YE2730A d_{33} METER).

Thermal expansion ($\Delta L/L$) and linear thermal expansion (α) were carried out using a specially designed measuring stand based on MICRON-02 end block testers, an Agilent 34420A nanovoltmeter/microohmmeter. The displacement sensitivity was 10^{-8} m, the measurement error was ~4%. The temperature in the chamber changed at a rate of ΔT =1 K/min.

3. Experimental Results and Discussion

3.1. *X-ray studies*

X-ray patterns of SS $(1-x)PbTi_{0.5}Zr_{0.5}O_3 - xCdNb_2O_6$ are shown in Fig. 1. All samples have a perovskite-type structure with a tetragonal (T) unit cell. A very small amount of ZrO_2 is contained in all samples, except for SS with x = 0.050. Figure 1 also shows the diffraction peaks 111 and the doublet 002, 200 corresponding to the tetragonal (T) distortion of the crystal lattice, enlarged along the 2θ axis. It can be seen that as x increases, the diffraction pattern degrades for all values of x, and the diffraction peaks are a superposition of several peaks. This means that SSs are inhomogeneous and consist of a series of T-phases with close cell parameters. Additionally, the background increases between peaks 002 and 200 in SS with x = 0.0250, 0.0375, 0.050, with the highest increase observed at x = 0.0375. The same effect takes place in the PZT system in the region of the morphotropic phase transition from the T-phase to the rhombohedral one and is associated with the appearance of intermediate monoclinic phases.

In the system under study, there is no change in the symmetry of the crystal lattice; therefore, the increase in the background between the 002 and 200 peaks may be due to the appearance of local regions (clusters) with a symmetry other than T.

Figure 2 shows the dependences of the structural parameters, the half-width of the diffraction peak (111), and the densities of the ceramics SS of the composition

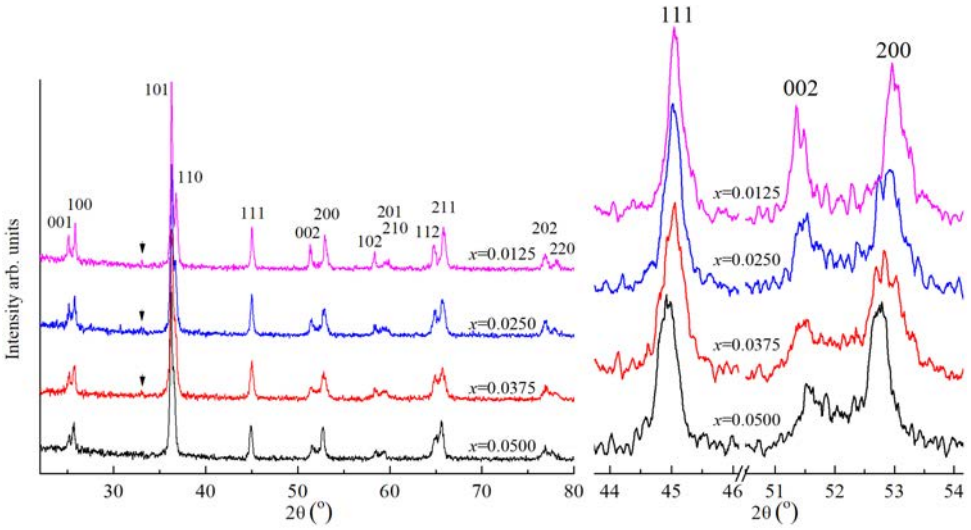

Fig. 1. X-ray diffraction patterns of $(1 - x)PbTi_{0.5}Zr_{0.5}O_3 - xCdNb_2O_6$ SSs in the range $2\theta = 22–80$ (°) (the arrow marks the ZrO_2 line) and diffraction reflections $(111)_k$, $(200)_k$ on a scale enlarged along the 2θ axis.

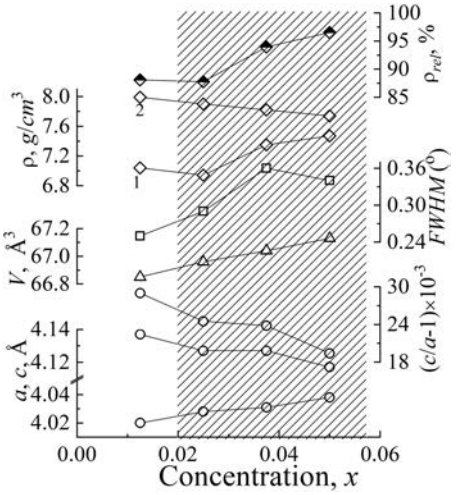

Fig. 2. Concentration dependences of parameters a, c, degree of distortion c/a, volume, V, tetragonal cell, half-width, B, diffraction peak (111), experimental (1), X-ray (2) and relative densities of SS ceramics of composition $(1–x)PbTi_{0.5}Zr_{0.5}O_3 – xCdNb_2O_6$.

$(1–x)PbTi_{0.5}Zr_{0.5}O_3 – xCdNb_2O_6$ (hatching highlights the field with coexisting local regions (clusters) with symmetry different from T-symmetry).

Unexpectedly, the dependence $V(T)$ manifests itself with a monotonic increase as the concentration of $CdNb_2O_6$ increases. The ionic radii A of the cations are as follows: Pb^{2+} = 1.411Å Cd^{2+} = 1.109Å at a coordination number of 12). It would seem that the volume of the unit cell should decrease during the formation of the substitutional SS. However, with heterovalent substitution, things are not as obvious. When an ion with a lower valence $(Ti/Zr)^{4+}$ is replaced by an ion with a higher valence Nb^{5+}, vacancies are formed in the B sublattice or intercalated anions appear. In both cases, the V cell should increase as a result of swelling of the cell vacancy or the interstitial atom. The maximum dependence of the half-width of the diffraction peak (B) on the (x)-single peak (111) corresponds to the maximum background between peaks 002, 200 and confirms the assumption that clusters of additional phases have a symmetry lower than T. Ceramic densities increase dramatically at $x > 0.025$, which is also typical of the SS of the $PbTi_{1-x}Zr_xO_3$ system in the morphotropic region.[11]

Therefore, by X-ray diffraction, it is shown that in the system $(1 - x)$ $PbTi_{0.5}Zr_{0.5}O_3 - xCdNb_2O_6$, in the range $0.0125 \le x \le 0.050$, inhomogeneous SSs are formed, the average - symmetry of which is preserved, but in the interval $0.0375 \le x \le 0.050$, clusters with lower symmetry appear. Note that the only condition preventing substitutional SS formation in $(1 - x)PbTi_{0.5}Zr_{0.5}O_3 - xCdNb_2O_6$ system is the nonisostructural nature of the extreme components (perovskite-columbite). The remaining conditions, such as the difference in ionic radii and the difference in the electronegativity of interchangeable elements, follow the rules of isomorphism.[12,13]

3.2. *Microstructure*

Figure 3 shows fragments of SS microstructures of the studied system with the content (x) of $CdNb_2O_6$: 0.0125 (a), 0.025 (b), 0.0375 (c), 0.050 (d). It is clearly seen that the grain landscape is represented by crystallites, the size, shape, and character of the packing of which change depending on the quantitative ratios of the components in the system. Therefore, when the latter is enriched with cadmium niobate, the average grain size, $\bar{D}$, decreases almost threefold with variation of $CdNb_2O_6$ in the range of $0.0125 \le x \le 0.050$. At the same time, the nature of the dependence $\bar{D}(x)$ (Fig. 4) is nonmonotonic with a fast change in $\bar{D}$ in the range $0.0125 <$

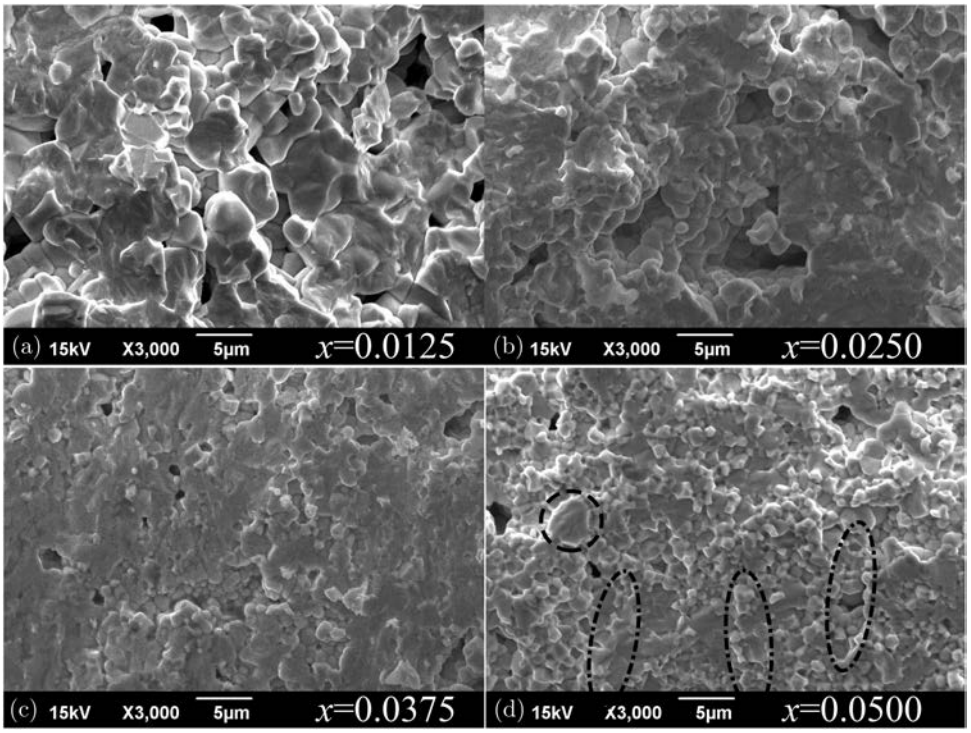

Fig. 3. Microstructure fragments of the studied SSs at different content of $CdNb_2O_6$ (x).

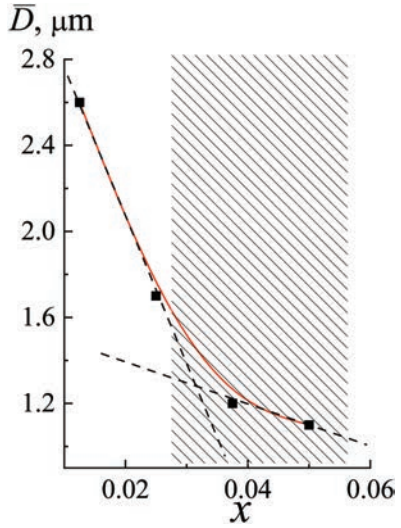

Fig. 4. Dependences of the average grain size $\bar{D}$ of ceramics of composition $(1-x)PbTi_{0.5}Zr_{0.5}O_3 - xCdNb_2O_6$ on the concentration of $CdNb_2O_6$ (x).

$x \le 0.025$, a gradually decreasing grinding rate $\bar{D}$ in the range $0.050 < x \le 0.075$ and slow decay of transformation speed $\bar{D}$ at $0.0375 < x \le 0.050$. The grain habit also changes as the system is saturated with a Cd-containing component: from crystallites with a mixed type of boundaries — curvilinear and close to rectilinear (x = 0.0125; 0.025) [Figs. 3(a) and 3(b)] to, basically, almost spheroidal grains at x = 0.0375; 0.50 [Figs. 3(c) and 3(d)]. Hence, in the latter case the sphericality of the grains sometimes turns out to be apparent because of their small size. Examination of the microstructure at high magnification shows that some of the grains retain the relative straightness of the boundaries in this case as well. The grain packing also undergoes changes: from loose at low concentrations of columbite to dense with large additions of $CdNb_2O_6$. In this case, in the latter case, in parallel with the main mass of grains of small size, single grains crystallize, much larger (by an order of magnitude) in size [Fig. 3(d), highlighted by hatching]. Texturization of the grain field manifested itself to the greatest extent at a higher concentration of $CdNb_2O_6$ [Fig. 3(d), "columns" of grains are highlighted with a dashed dotted line].

The observed results can be explained as follows. As evidenced by the above X-ray data, all SSs of this system are very inhomogeneous and represent series of T-phases with close cell parameters, and at $x \ge 0.025$, in addition to them, they probably also contain structures with a symmetry other than T-symmetry. It is quite obvious that, against the background of such structural instability, one should not expect the formation of an ideal grain pattern with close-packed crystallites characterized by perfect faceting. Additionally, the complication of phase filling of SS as $CdNb_2O_6$ is introduced into the system naturally slows recrystallization processes, slowing grain growth, which is what we observe in practice. At the same time, as can be seen from Fig. 3, the transition to a highly refined grain landscape occurs precisely in the concentration range where, in our opinion, phases with a symmetry other than T-symmetry are formed. It is very

likely that its region of existence extends below room temperature (which requires additional X-ray studies), similar to how it occurs in the known binary PZT system (Pb(Zr, Ti)O_3) in the morphotropic region (rhombohedral-tetragonal), in which the monoclinic phase appears.[14,15] The appearance of directional "columns", grains (packing textures), apparently, is associated both with the action of applied pressure during ceramic sintering and the presence of a nonisostructural component ($CdNb_2O_6$), which is associated with deformations of the crystalline cell of the base SS, which contribute to some extent to the formation of packaging textures.

The appearance at x=0.0500 in the grain structure of crystallites, which are much larger than most grains, may be a consequence of the appearance of a liquid phase during the synthesis and sintering of the corresponding ceramics, which provokes abnormal growth of secondarily recrystallized grains.[16,17] Its source can be various intermediate media containing Cd, Pb, and Nb with low melting points.[18,19]

3.3. *Electrophysical properties*

Figure 5 shows the results of a study of the dielectric, piezoelectric and ferroelastic properties of the composition of SS $(1 - x)PbTi_{0.5}Zr_{0.5}O_3 - xCdNb_2O_6$ at T = 300K. It is shown that an increase in the content of $CdNb_2O_6$ to $x < 0.0375$ does not cause any significant changes in the dielectric properties. The piezoelectric characteristics of the studied samples change on average by ~60%. Elastic constants experience the most significant fluctuations, that is, Q_M increases by ~2.5 times, while Y_{11}^E and V_1^E change by ~80%. It can be seen that an increase in the content of $CdNb_2O_6$ in the system leads to nonmonotonic changes in all the presented characteristics, most noticeable in the concentration field (highlighted in Fig. 5 by hatching) where, in our opinion, (clusters) appear with a symmetry other than T-symmetry.

3.4. *Dielectric spectroscopy*

Figures 6–9 show dependences $\varepsilon'/\varepsilon_0|_f(a)$, $\varepsilon''/\varepsilon_0(b)$ ($f = 25 \div 2 \times 10^6$ Hz), $\varepsilon'/\varepsilon_0$ (in heating/cooling mode), $(\varepsilon'/\varepsilon_0)^{-1}$ (f = 840512 Hz) (T) (c) of the studied ceramics, in the temperature range T = (300–800)K.

It can be seen that the dependences $\varepsilon'/\varepsilon_0(T)$ [Figs. 6–9(a) have an λ-shaped form with clear maxima that do not blur and do not change position with increasing frequency of the alternating electric field (f). The presented dependences are characterized by the absence of the dispersion $\varepsilon'/\varepsilon_0$ to the left of the Curie temperature (T_C), its appearance at the moment of phase transition (PT) and to the right of T_C. Above T_C, a rapid increase in $\varepsilon'/\varepsilon_0$ is revealed, starting from temperatures that are lower, the lower f.

Curves $\varepsilon''/\varepsilon_0$ (T) [Figs. 6–9(b) are characterized by the presence of a plateau-like section that precedes the phase transition to the paraelectric (PE) phase, in which $\varepsilon''/\varepsilon_0$ either increases slightly or remains constant, giving way to a sharp increase near T_C. All of the above is characteristic of classical ferroelectrics.

Studies of dependences $(\varepsilon'/\varepsilon_0)^{-1}$ on temperature [Fig. 6(c) showed that the objects analyzed in the PE phase obey the empirical Curie–Weiss law, $\varepsilon'/\varepsilon_0 - 1 = C/(T - T_C)$, where C is the Curie–Weiss constant, T_C is the Curie–Weiss temperature.

An increase in dispersion $\varepsilon'/\varepsilon_0$ in the PE phase against the background of a sharp increase in $\varepsilon''/\varepsilon_0$ can be associated with an increase in the electrical conductivity of the material, in particular, due to the release of bound charges involved in the detection of spontaneous polarization in the FE phase, and

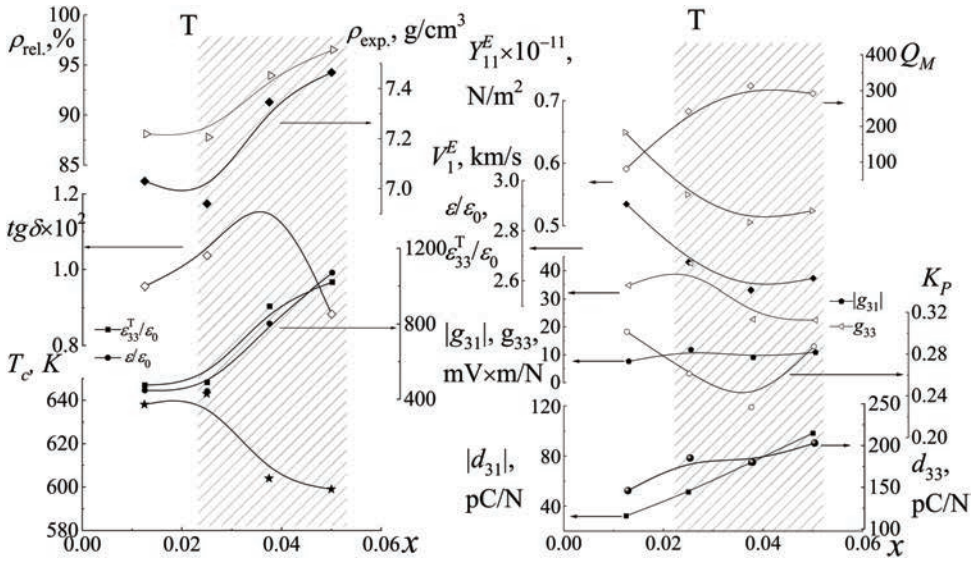

Fig. 5. Dependences of the dielectric, piezoelectric and ferroelastic characteristics of the SS composition $(1 - x)PbTi_{0.5}Zr_{0.5}O_3 - xCdNb_2O_6$ on the content of $CdNb_2O_6$ (x) in the system (T = 300K).

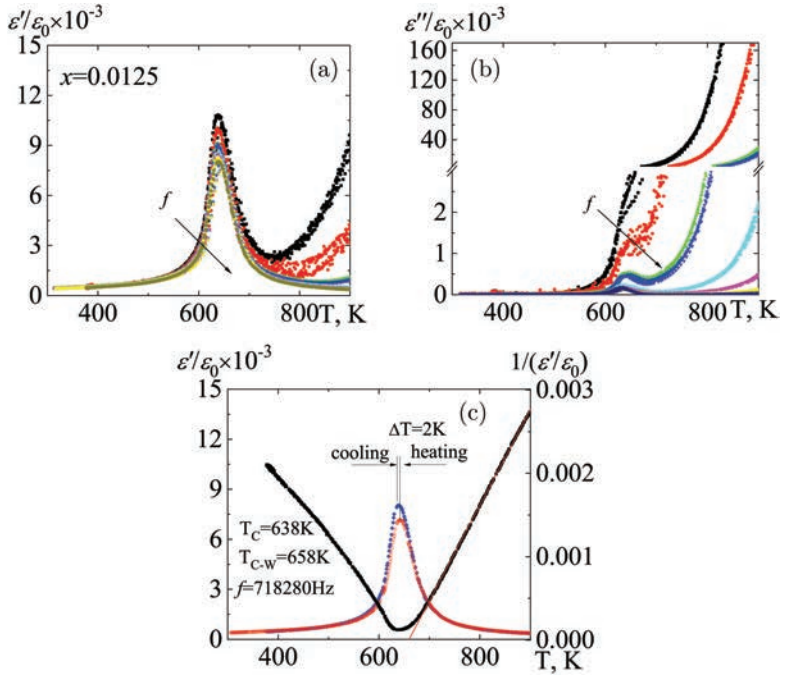

Fig. 6. Dependences $\varepsilon'/\varepsilon_0$, $\varepsilon''/\varepsilon_0$, $(\varepsilon'/\varepsilon_0)^{-1}(T)$ at $f \sim$ (0.0005– 1.2) MHz of SS $(1-x)PbTi_{0.5}Zr_{0.5}O_3 - xCdNb_2O_6$ ceramics with x = 0.0125, in the range T = (300–900)K.

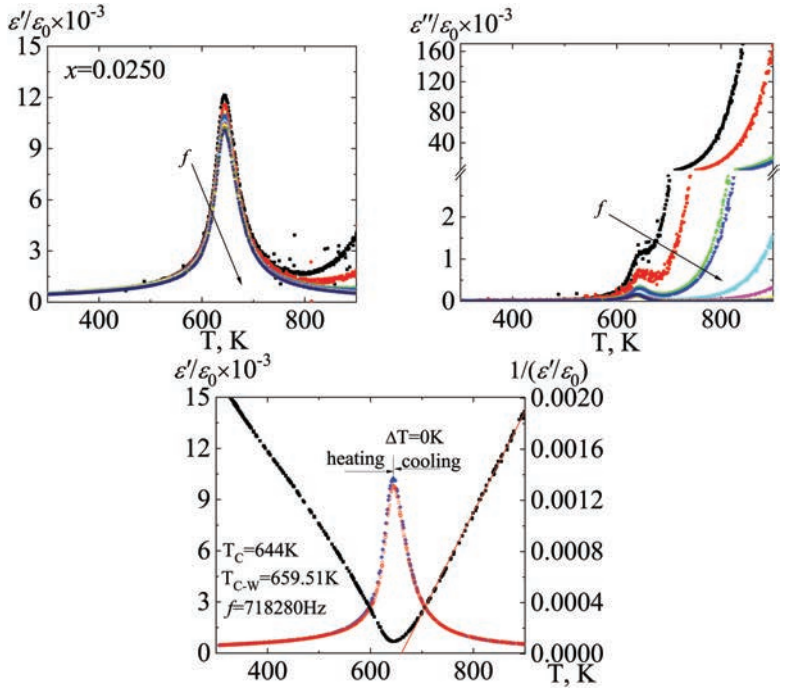

Fig. 7. Dependences $\varepsilon'/\varepsilon_0$, $\varepsilon''/\varepsilon_0$, $(\varepsilon'/\varepsilon_0)^{-1}$(T) at $f \sim$ (0.0005 – 1.2) MHz of SS $(1-x)PbTi_{0.5}Zr_{0.5}O_3 - xCdNb_2O_6$ ceramics with x = 0.0250, in the range T = (300–900)K.

also due to the appearance of vacancies during redox processes of ions of variable valence (Ti, Nb).

All studied SS are characterized by the presence of three sections characterized by different rates of change in piezoelectric characteristics: ~(300–480)K, ~(480–580) K and ~(580–660)K (depending on x). The first is characterized by the formation of an extremum of the studied dependences, the second at $x < 0.0500$ is characterized by an

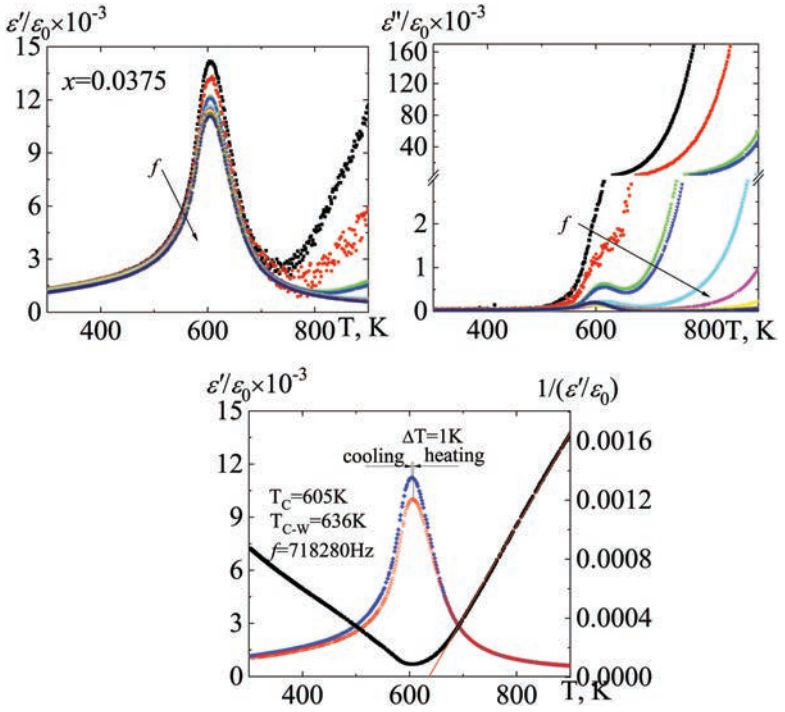

Fig. 8. Dependences $\varepsilon'/\varepsilon_0$, $\varepsilon''/\varepsilon_0$, $(\varepsilon'/\varepsilon_0)^{-1}(T)$ at $f \sim (0.0005 - 1.2)$ MHz of SS $(1-x)PbTi_{0.5}Zr_{0.5}O_3 - xCdNb_2O_6$ ceramics with $x = 0.0375$, in the range $T = (300–900)$K.

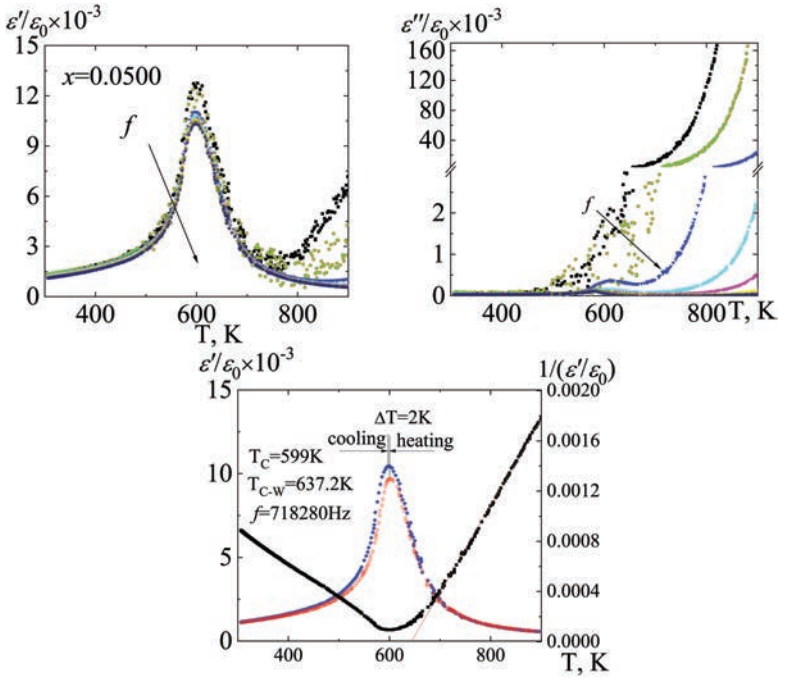

Fig. 9. Dependences $\varepsilon'/\varepsilon_0$, $\varepsilon''/\varepsilon_0$, $(\varepsilon'/\varepsilon_0)^{-1}(T)$ at $f \sim (0.0005 - 1.2)$ MHz of SS $(1-x)PbTi_{0.5}Zr_{0.5}O_3 - xCdNb_2O_6$ ceramics with $x = 0.0500$, in the range $T = (300–900)$K.

increase in the rate of change of the studied characteristics, and SS with $x = 0.0500$ is characterized by the formation of two extrema of the studied piezoelectric characteristics. In the third region, an anomalously sharp change in parameters was revealed as the Curie point approached all concentrations of $CdNb_2O_6$.

Figure 10 shows the dependences of dielectric, electrophysical, ferroelastic and thermophysical characteristics on

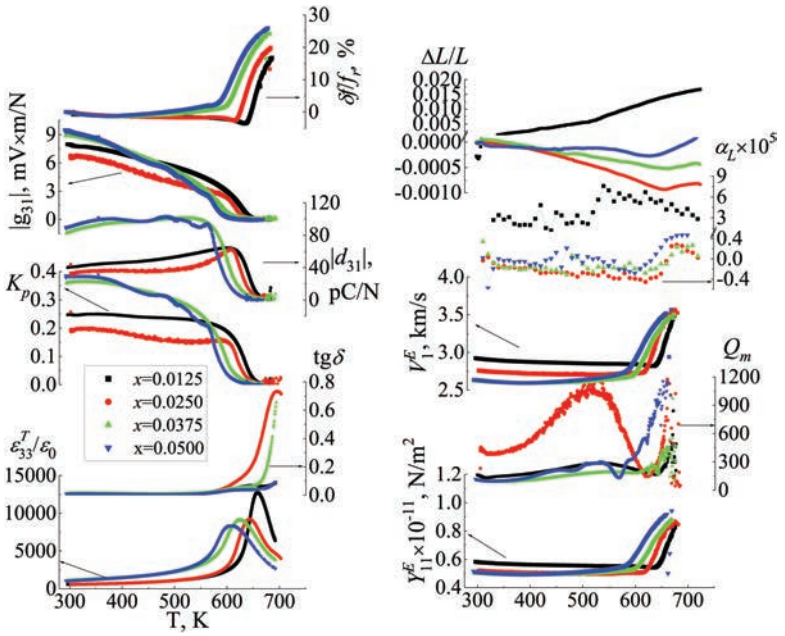

Fig. 10. Dependences of dielectric, electrophysical, ferroelastic, and thermophysical characteristics on the TR temperature $(1-x)$-$PbTi_{0.5}Zr_{0.5}O_3 - xCdNb_2O_6$ with different content of $CdNb_2O_6$, in the range $T = (300–900)$K.

the temperature of SS with different content of $CdNb_2O_6$ at $T = (300–740)$K. The ferroelastic properties demonstrate a similar behavior, but the features described above are not so pronounced. An exception is the $Q_M(T)$ dependence. It is also necessary to single out the SS with $x = 0.0250$, in which the specified dependence $Q_M(T)$ varies in a fairly wide range of values.

The study of thermophysical properties revealed several features. Therefore, the formation of extrema of dependences $(\Delta L/L,\ \alpha)(T)$ correlates with the manifestation of such anomalies in the electrophysical characteristics. In an SS with $x = 0.0125$, $\Delta L/L$ increases as the temperature increases. At $x > 0.0125$, $\Delta L/L$ decreases with the temperature of the transition to the paraelectric phase; a further increase is accompanied by an increase in this characteristic. It should also be noted that an increase in the content of $CdNb_2O_6$ causes a decrease in the rate of change in $\Delta L/L$ with increasing temperature.

The formation of extrema in the studied dependences of piezoelectric characteristics on temperature (Fig. 10) indicates the presence of structural instabilities that are present in the base SS of the composition of $PbZr_{0.5}Ti_{0.5}O_3$.[20] The abrupt change in characteristics in the vicinity of T_C is most likely due to the processes of depolarization of objects resulting from the transition to a nonpolar cubic phase, and the persistence of a weak piezoresponse in a narrow temperature range after this transition is probably due to the presence of polar regions that have a piezoresponse similar to the same effect in ferroelectric relaxors.

The implementation of a positive thermal expansion coefficient in the studied SS with $x = 0.0125$ is traditional and is associated with an increase in unit cell volume with increasing temperature. However, the manifestation of a negative coefficient of thermal expansion (NTE) in SS with $x > 0.0125$ is quite unusual. This phenomenon has been discussed in many publications, and there are several points of view on this subject related to phase transitions, transverse phonon vibrations, single hard modes, and specific sample morphology.[21,22] In our opinion, in this case, the occurrence of a crystal chemical disorder in SS as a result of the appearance of T-phases with similar unit cell parameters is decisive, which can lead to a decrease in the cell volume at low concentrations of cadmium niobate and the formation of a certain composite state. This can reduce the length of the B–O and A–O bonds during the C→T phase transition and, as a result, reduce the volume of the unit cell.[23] The decrease in negative thermal expansion with increasing $CdNb_2O_6$ content may be due to the possibility of placing Cd and Nb cations in irregular $CdNb_2O_6$ positions, and as a result of the occurrence of a stronger disorder, which reduces the contribution of short bonds to the resulting volume. However, further studies are required to confirm the above assumptions.

3.5. *Phase transition fatigue*

The thermally induced aging of ceramics was studied using data from dielectric spectroscopy, taking into account the established concepts of factors responsible for the smearing of phase transitions. Figures 11–14 show the change in the parameters T_C, T_A, ε_A, and δ_A with an increasing number of cycles (n) passing through the Curie point, calculated from

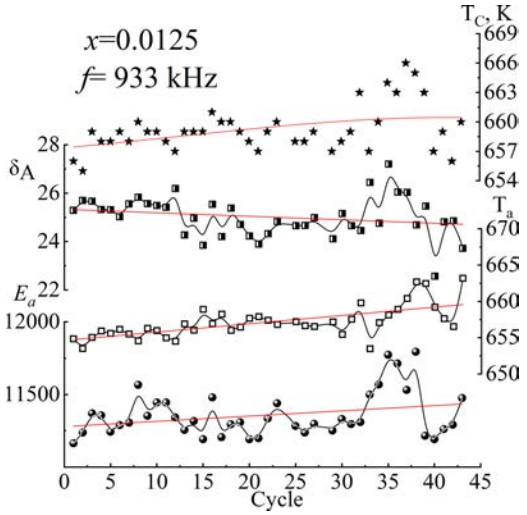

Fig. 11. Dependences of the Curie temperature (T_c) and the parameters of the empirical law [formula 1] for ceramics SS $(1-x)Pb(Ti_{0.5}Zr_{0.5})O_3–xCdNb_2O_6$ with $x = 0.0125$ on the number of cycles.

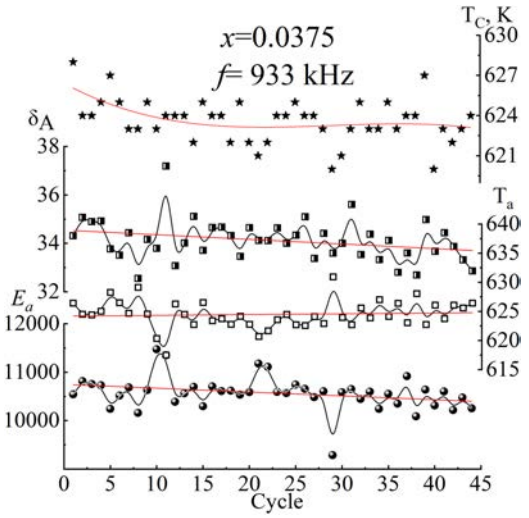

Fig. 13. Dependences of the Curie temperature (T_c) and the parameters of the empirical law [formula 1] for ceramics SS $(1-x)Pb(Ti_{0.5}Zr_{0.5})O_3–xCdNb_2O_6$ with $x = 0.0375$ on the number of cycles.

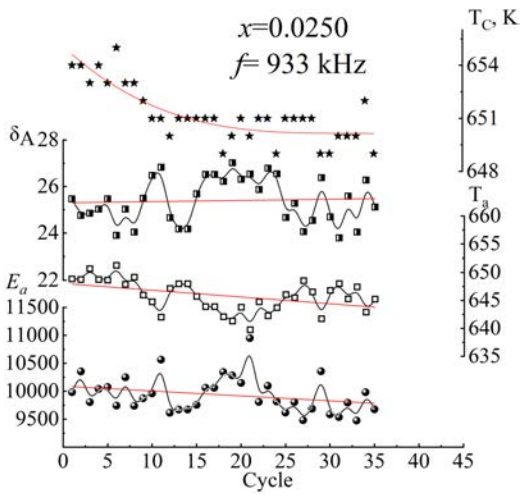

Fig. 12. Dependences of the Curie temperature (T_c) and the parameters of the empirical law [formula 1] for ceramics SS $(1-x)Pb(Ti_{0.5}Zr_{0.5})O_3–xCdNb_2O_6$ with $x = 0.0250$ on the number of cycles.

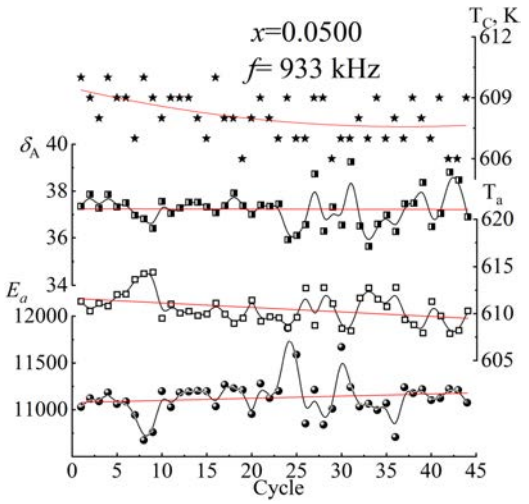

Fig. 14. Dependences of the Curie temperature (T_c) and the parameters of the empirical law [formula 1] for ceramics SS $(1-x)Pb(Ti_{0.5}Zr_{0.5})O_3–xCdNb_2O_6$ with $x = 0.0500$ on the number of cycles.

the dependences $\varepsilon'/\varepsilon_0(T)$ measured at a frequency of 933 kHz, for SS with different concentrations of $CdNb_2O_6$.

Analysis of the obtained data confirms the previously proposed classification and allows us to divide the objects studied into two groups. The first includes a sample with $x = 0.0125$, in which the indicated parameters remain stable up to 30 cycles, while the temperatures T_C and T_A increase monotonically, δ_A also decreases monotonically, and ε_A remains almost unchanged. The second group includes SSs with $x > 0.0125$, which are characterized by a decrease in T_C during the first 10–15 cycles with subsequent stabilization.

The calculated parameters, including the blur parameter δ_A, experience anomalies in the same region in the form of sharp jumps with the formation of local extrema. It can be assumed that the defects and/or the low-symmetry clusters mentioned above are ordered in this region. In general, the parameters considered for this group of SS experience a fairly wide spread of values, which, of course, is a consequence of the complication of phase filling of these objects as $CdNb_2O_6$ is introduced into the system, and therefore it becomes difficult to unambiguously establish the trend of their change during thermal cycling.

We only note that the smallest scatter of parameters in this group is typical for SS with $x = 0.0500$, which is apparently due to the presence of a liquid phase here, which provokes a stabilizing effect.

4. Conclusions

For the first time, solid phase synthesis followed by sintering using conventional ceramic technology was used to obtain SS samples of the three-component system $(1-x)Pb(Ti_{0.5}Zr_{0.5})O_3-xCdNb_2O_6$ with $x = 0.0125 \div 0.0500$, $\Delta x = 0.0125$.

X-ray diffraction analysis showed that samples with $x = 0.0125$ have a perovskite-type structure with a tetragonal unit cell. At $x > 0.0125$, SSs are inhomogeneous and consist of a series of T-phases with close cell parameters.

The grain landscape has been established to be represented by crystallites, the size, shape, and nature of the packing changes depending on the quantitative ratios of the components in the system, and the average grain size decreases by almost a factor of three when $CdNb_2O_6$ varies in the range $0.0125 \le x \le 0.050$. An explanation of the observed effect is given.

The results of the study of dielectric spectroscopy showed that the dependences $\varepsilon'/\varepsilon_0(T)$ have a λ-shaped form with clear maxima that do not blur and do not change position with an increase in the frequency of the alternating electric field (f), and in the paraelectric phase they obey the empirical Curie–Weiss law. This indicates that all investigated SSs are classical ferroelectrics.

It has been established that the electrophysical characteristics during heating to the transition to the paraelectric state are characterized by three sections, with different rates of their change: ~(300–480)K, ~(480–580)K, and ~(580–660) K (depending on x). The study of thermophysical properties revealed the formation of extrema of dependences ($\Delta L/L$, α) (T), which correlate with the manifestation of similar anomalies in electrical characteristics. At $x > 0.0125$, $\Delta L/L$ decreases to the transition temperature to the paraelectric phase.

An analysis of thermally induced aging made it possible to establish that, in SS with $x = 0.0125$, the dielectric parameters remain stable up to 30 cycles. With an increase in the $CdNb_2O_6$ content, SS are characterized by a decrease in T_C during the first 10–15 cycles with subsequent stabilization, and the smearing parameter, δ_A, experiences anomalies in the form of sharp jumps with the formation of local extrema. The smallest scatter of parameters is typical for SS with $x = 0.0500$, which is probably due to the presence of a liquid phase, which provokes a stabilizing effect.

The data obtained should be used in the development of similar materials and devices based on them.

Acknowledgments

The study was carried out with the financial support of the Ministry of Science and Higher Education of the Russian Federation (State task in the field of scientific activity, scientific project No. (0852-2020-0032)/(BAZ0110/20-3-07IF). The equipment of the Center of Research Institute of Physics SFedU, "High-Tech" SFedU was used. This report is presented at the 10th Anniversary International Conference on "Physics and Mechanics of New Materials and Their Applications" (PHENMA 2021), Divnomorsk, Russia, May 23–27, 2022.

References

[1]D. Berlincourt, *Ultrasonic Transducer Materials. Ultrasonic Technology,* eds. O. E. Mattiat, Chapter 2 (Springer, Boston, MA, 1971), pp. 63–124. https://doi.org/10.1007/978-1-4757-0468-6_2.

[2]B. Jaffe, *Piezoelectric Ceramics* (Academic Press, London, UK, 1971).

[3]I. N. Andryushina, L. A. Reznichenko, I. M. Shmytko, L. A. Shilkina, K. P. Andryushin, Y. I. Yurasov and S. I. Dudkina, The PZT system ($PbTi_xZr_{1-x}O_3$, $0 \le x \le 1.0$): Dielectric response of solid solutions in broad temperature. ($10 \le T \le 1000$ K) and frequency ($10^{-2} \le f \le 10^7$ Hz) ranges (Part 4) *Ceram. Int.* **39**, 3979 (2013). https://doi.org/10.1016/j.ceramint.2012.10.246.

[4]B. Lewis and E. A. D. White,. Lxv. Structure and phase transitions of ferroelectric sodium cadmium niobates, *J. Electronics Control* **1**, 646 (1956). https://doi.org/10.1080/00207215608961468.

[5]W. N. Lawless, Specific heats of lead and cadmium niobates at low temperatures, *Phys. Rev. B* **19**, 3755 (1979). https://doi.org/10.1103/PhysRevB.19.3755.

[6]Y.-J. Hsiao, T.-H. Fang, L.-W. Ji and S.-S. Chi, Surface and photoluminescence characteristics of $CdNb_2O_6$ nanocrystals, *Open Surf. Sci. J.* **1**, 30 (2014). https://doi.org/10.2174/18765319009010100 30.

[7]Y. J. Hsiao, Y. S. Chang, G. J. Chen and Y. H. Chang, Synthesis and the luminescent properties of $CdNb_2O_6$ oxides by sol-gel process, *J. Alloys Compd.* **471**, 259 (2009). https://doi.org/10.1016/j.jallcom.2008.03.081.

[8]A. A. Bokov and Z. G. Ye, Phenomenological description of dielectric permittivity peak in relaxor ferroelectrics, *Solid State Commun.* **116**, 105 (2000). https://doi.org/10.1016/S0038-1098(00)00295-7.

[9]A. A. Pavelko, A. V. Pavlenko and L. A. Reznichenko, Effect of lithium carbonate modification on the ferroelectric phase transition diffusion in lead ferroniobate ceramics, *J. Adv. Dielectrics* **12**, 1 (2022). doi: 10.1142/S2010135X21600213.

[10]IEEE Standard on Piezoelectricity ANSI/IEEE Std 176-1987, New York. 1988. DOI: 10.1109/IEEESTD.1988.79638.

[11]I. N. Andryushina, L. A. Reznichenko, L. A. Shilkina, K. P. Andryushin and S. I. Dudkina, The PZT system ($PbTi_xZr_{1-x}O_3$, $0 \le x \le 1.0$): The real phase diagram of solid solutions (room temperature) (Part 2), *Ceram.* Int. **39**, 1285 (2013). https://doi.org/10.1016/j.ceramint.2012.07.060.

[12]P. Gopalan and B. Kahr, Reevaluating structures for mixed crystals of simple isomorphous salts, $Ba_xPb_{1-x}(NO_3)_2$, *J. Solid State Chem.* **107**, 563 (1993). https://doi.org/10.1006/jssc.1993.1382.

[13]V. S. Urusov and N. N. Eremin, Local structure of solid solutions from the computer simulation results and experimental data, *J. Struct. Chem.* **56**, 737 (2015). https://doi.org/10.1134/S0022476615040186.

[14]B. Noheda, D. E. Cox, G. Shirane, J. A. Gonzalo, L. E. Cross and S. E. Park, A monoclinic ferroelectric phase in the $Pb(Zr_{1-x}Ti_x)O_3$ solid solution, *Appl. Phys. Lett.* **74**, 2059 (1999). https://doi.org/10.1063/1.123756.

[15]B. Noheda, J. A. Gonzalo, R. Guo, S. E. Park, L. E. Cross, D. E. Cox and G. Shirane, The monoclinic phase in PZT: New light on morphotropic phase boundaries, *AIP Conf. Proc.* **535**, 304 (2000). https://doi.org/10.1063/1.1324468.

[16]P. Bomlai, Sintering, microstructure and electrical properties of MnO_2 and CuO doped $[Na_{0.515}K_{0.485}]_{0.94}Li_{0.06}(Nb_{0.99}Ta_{0.01})$-

O_3 ceramics, *Adv. Mater. Res.* **770**, 258 (2013). https://doi.org/10.4028/www.scientific.net/AMR.770.258.

[17]P. Bomlai, N. Muensit and S. J. Milne, Structural and electrical properties of (1-x)($Na_{0.465}K_{0.465}Li_{0.07}$)$NbO_3$- x$CaTiO_3$ lead-free piezoelectric ceramics with high Curie temperature, *Procedia Eng.* **32**, 814 (2012). https:doi:10.1016/j.proeng.2012.02.017.

[18]R. S. Roth, Phase equilibrium relations in the binary system lead oxide-niobium pentoxide, *J. Res. National Bureau Standards* **62**, 27 (1959). http://dx.doi.org/10.6028/jres.062.006.

[19]R. S. Roth, Phase equilibria in the system cadmium oxide-niobium oxide, *J. Am. Ceram. Soc.* **44**, 49 (1961). doi:10.1111/j.1151-2916.1961.tb15347.x.

[20]I. N. Andryushina, L. A. Reznichenko, L. A. Shilkina, K. P. Andryushin and S. I. Dudkina, The PZT system ($PbTi_xZr_{1-x}O_3$, $0 \le x \le 1.0$): High temperature X-ray diffraction studies. Complete x-T phase diagram of real solid, *Ceram. Int.* **39**, 2889 (2013). https://doi.org/10.1016/j.ceramint.2012.09.063.

[21]J. S. O. Evans, Negative thermal expansion materials, *J. Chem. Soc. Dalton Trans.* **19**, 3317 (1999). https://doi.org/10.1039/a904297k.

[22]P. J. Attfield, Mechanisms and materials for NTE, *Front. Chem.* **6**, 1 (2018). https://doi.org/10.3389/fchem.2018.00371.

[23]A. Chandra, D. Pandey, M. D. Mathews and A. K. Tyagi, Large negative thermal expansion and phase transition in ($Pb_{1-x}Ca_x$)TiO_3 ($0.30 \le x \le 0.45$) ceramics, *J. Mater. Res.* **20**, 350 (2005). https://doi.org/10.1557/JMR.2005.0062.